MATERIALS CHEMISTRY
FRONTIERS

RESEARCH ARTICLE

View Article Online
View Journal | View Issue

Cite this: *Mater. Chem. Front.*, 2020, **4**, 1764

Synergy of PVP and ethanol to synthesize Ni_3S_4 quantum dots for high-performance asymmetric supercapacitors†

Jinfeng Zheng,[a] Xiao Lian,[a] Mingzai Wu,[b] Fangcai Zheng,[c] Yuanhao Gao[d] and Helin Niu *[a]

Received 1st April 2020,
Accepted 18th April 2020

DOI: 10.1039/d0qm00201a

rsc.li/frontiers-materials

Ni_3S_4 quantum dots (QDs) have great potential for supercapacitors due to their unique quantum effects, high specific surface area, high water solubility and good stability, but the current preparation process is cumbersome and toxic. Here, we highlight a facile and environmentally-friendly synthesis of Ni_3S_4 QDs for the first time by virtue of the synergy of polyvinylpyrrolidone (PVP) and ethanol. The synergistic mechanism was revealed by using XRD to investigate the effect of the synthesis solvent. When QDs were used as a supercapacitor electrode material they exhibited excellent electrochemical properties, and the specific capacitance at 1 A g^{-1} was 1440 F g^{-1}. In addition, Ni_3S_4 QDs and activated carbon (AC) are assembled into a Ni_3S_4 QD//AC asymmetric supercapacitor (ASC), which delivered a maximum energy density of 60.4 W h kg^{-1}. This work provides new ideas for the preparation of QDs and opens up new concepts for the synthesis of nickel sulfide.

1. Introduction

In the fields of mobile electronic devices and hybrid vehicles, the demand for energy and electricity has witnessed a continuous increase, which has triggered a boom in the research of electrode materials for advanced energy storage equipment, for instance, lithium-ion batteries and supercapacitors.[1] Among various energy storage devices, lithium-ion batteries have greatly improved people's lives and have recently won the Nobel Prize.[2,3] However, they suffer from low power density, while supercapacitors can provide high power in an instant, and also have a higher energy density than a conventional dielectric capacitor.[4,5]

It is well known that the capacitance and charge storage capacity of supercapacitors are highly dependent on the nature of the electrode material. Currently, various types of electrode materials have been studied, such as sulfides,[6,7] oxides,[8,9] hydroxides,[10] polymers[11] and carbon materials.[12] Among various electrode materials, transition metal sulfides have been extensively studied due to their unique chemical and physical properties.[13] Among them, Ni_3S_4 is favored by researchers for its higher theoretical specific capacitance and good rate performance.[14] In addition, due to the rich sources and low price of Ni_3S_4, it can meet the increasing demand of energy storage systems. Although various morphologies of Ni_3S_4 have been studied as electrode materials for supercapacitors such as rose,[15] polyhedron[16] and composite materials,[17] their performance needs to be further improved.

For supercapacitors, the structure and morphology of electrode materials have a very important influence on their capacitance performance. Increasing the specific surface area of the material can enhance the redox reaction between the active material and the electrolyte.[18] With the dimensionality reduced to zero, the proportion of atoms exposed on the surface of the QDs increases. Because the surface atom coordination is insufficient, the surface atom activity increases. These highly active surface atoms have a significant effect on the properties of the QDs, such as high catalytic activity, and strong reduction and oxidation.[19–21] Making nickel sulfide into QDs can improve the electrochemical performance, including increasing the specific surface area, improving the electrochemical activity, and giving more charge transport routes. Preparation of nickel sulfide QDs has been reported, which usually involves toxic solvents and requires complex nitrogen protection and injection, for example, NiS_2 QDs synthesized in oleylamine, which demands a nitrogen atmosphere,[22] and Ni_3S_4 QDs synthesized in ethylene

[a] *Anhui Province Key Laboratory of Chemistry for Inorganic/Organic Hybrid Functionalized Materials, Institutes of Physical Science and Information Technology, Key Laboratory of Structure and Functional Regulation of Hybrid Materials of Ministry of Education, Anhui University, Hefei 230601, China. E-mail: niuhelin@ahu.edu.cn*
[b] *School of Physics and Materials Science, Anhui University, Hefei 230039, China*
[c] *Institutes of Physical Science and information Technology, Anhui University, Hefei 230039, China*
[d] *Key Lab Micronano Mat Energy Storage, Xuchang University, Xuchang 461000, China*

† Electronic supplementary information (ESI) available. See DOI: 10.1039/d0qm00201a

glycol;[23] NiS_2 QD–C_3N_4 composite materials have also been synthesized, but this method cannot synthesize pure NiS_2 QDs.[24] Therefore, developing a simple and environmentally-friendly synthetic method will promote the application of nickel sulfide QDs in supercapacitors.

The particles reduce the mutual contact between themselves by electrostatically adsorbing a surfactant, thereby reducing the size of the product. Common neutral surfactant PVP has good biocompatibility, and is non-toxic and harmless and widely used in many fields. Because the unpaired electrons of the nitrogen atom in PVP participate in the pyrrole ring conjugated system, the electron cloud is biased toward the oxygen atom, so the nitrogen atom is weakly positively charged.[25] Not only does the nitrogen atom weaken the formation of hydrogen bonds, but it can also adsorb on negatively charged materials. At the same time, due to the long molecular chain of PVP, it has a good dispersion effect on the adsorbed material.

To put the above proposal into practice, PVP-induced Ni_3S_4 QDs were synthesized in a facile and environmentally-friendly fashion in one step. A mixed solution of water and ethanol was used as the solvent without the need for nitrogen protection and injection. The prepared Ni_3S_4 QDs exhibited a high specific capacitance of 1440 F g^{-1} at 1 A g^{-1}. In addition, the assembled Ni_3S_4//AC-ASC exhibited an energy density of 60.4 W h kg^{-1} at a power density of 400 W kg^{-1}. In the end, the device was successfully used in practice, and an LED was lit. This work demonstrates that Ni_3S_4 QDs can be used as an excellent supercapacitor electrode material and provides a simple and environmentally friendly new method for preparing QDs.

2. Experimental

2.1. Synthesis of Ni_3S_4 QDs

The reagents used were of analytical grade and were used without treatment. 3 mmol $NiCl_2{\cdot}6H_2O$, 4 mmol $Na_2S_2O_3{\cdot}5H_2O$, 15 mmol urea, and 0.5 g PVP (K-30) were dissolved in 20 mL of distilled water and ultrasonically assisted to dissolve, and then 20 mL of absolute ethanol was added and stirred uniformly. The mixed solution was transferred to a 50 mL round bottom flask and magnetically stirred, and then heated in an oil bath at 120 °C for 6 h. The small amount of air remaining in the flask is negligible. After that, the flask was taken out and cooled in cold water. We added 80 mL of acetone to the product solution and let it stand for 8 h to allow the Ni_3S_4 QDs to precipitate naturally. Thereafter, the supernatant was slowly poured out, 20 mL of distilled water was added, and the precipitate was uniformly dispersed by ultrasonic waves. We added another 50 mL of acetone and let it stand for 8 h to precipitate. The Ni_3S_4 QDs were cleaned 5 times in this way, and finally placed in a 60 °C vacuum drying oven for 12 h (the product is labeled P1).

In order to explore the formation mechanism of Ni_3S_4 QDs, we changed the solvent (20 mL water and 20 mL ethanol) to 40 mL of water. The other reaction conditions remained unchanged, and the synthesized product was labeled as P2.

2.2. Material characterization

The crystal structure was determined by X-ray diffraction (XRD, 9 kW/SmartLab, Japan). The elemental valence state was analyzed by X-ray photoelectron spectroscopy (XPS, 250Xi/ESCALAB, USA). The morphological structure was obtained by transmission electron microscopy (TEM, JEM-2100, Japan) and scanning electron microscopy (SEM, HITACHI S-4800, Japan). The surface area and pore size distribution of the product are measured by BET (Autosorb-IQ, USA).

2.3. Electrochemical measurements

Preparation of the working electrode. The prepared electrode material, acetylene black, and polytetrafluoroethylene (PTFE) were mixed at a mass ratio of 7 : 2 : 1 to prepare a film with a thickness of about 0.1 mm, and dried at 60 °C for 5 hours. The film was fixed on nickel foam with a tableting machine.[26] The weight of active material is about 2 mg. Each electrode had a geometric surface area of about 1 cm^2.

Electrochemical performance test. We used the electrode material, AC (Vulcan XC-72 carbon, USA) and a Hg/HgO electrode as a working electrode, counter electrode and reference electrode, tested in 6 M KOH. Electrochemical testing was performed on a Chenhua CHI660E electrochemical workstation and cycling stability testing was performed on a LAND CT2001A.

The specific capacitance of the electrode material can be calculated based on eqn (1):[27]

$$C_s = \frac{I \times \Delta t}{m \times \Delta V} \quad (1)$$

where C is the specific capacitance in F g^{-1}; I is the discharge current in A g^{-1}; t is the discharge time in s; m is the mass of the electrode material in g; and ΔV is the voltage difference in V.

The mass ratio of the positive and negative materials of the asymmetric capacitor is calculated by eqn (2) to ensure charge balance:[28]

$$R = \frac{m_+}{m_-} = \frac{C_- \cdot \Delta V_-}{C_+ \cdot \Delta V_+} \quad (2)$$

The following equation calculates the energy density (E) and power density (P):[29]

$$E = \frac{C \times \Delta V^2}{7200} \quad (3)$$

$$P = \frac{E \times 3600}{\Delta t} \quad (4)$$

where E is the energy density (W h kg^{-1}) and P is the power density (W kg^{-1}).

3. Results and discussion

3.1. Structure and morphology

The as-obtained P1 (in water and ethanol mixed solvent) and P2 (in water medium) were firstly characterized by XRD, which is exhibited in Fig. 1a. Clearly, as compared to the standard PDF card, it can be seen that P1 is Ni_3S_4 and P2 is $Ni_2(OH)_2(CO_3)$.

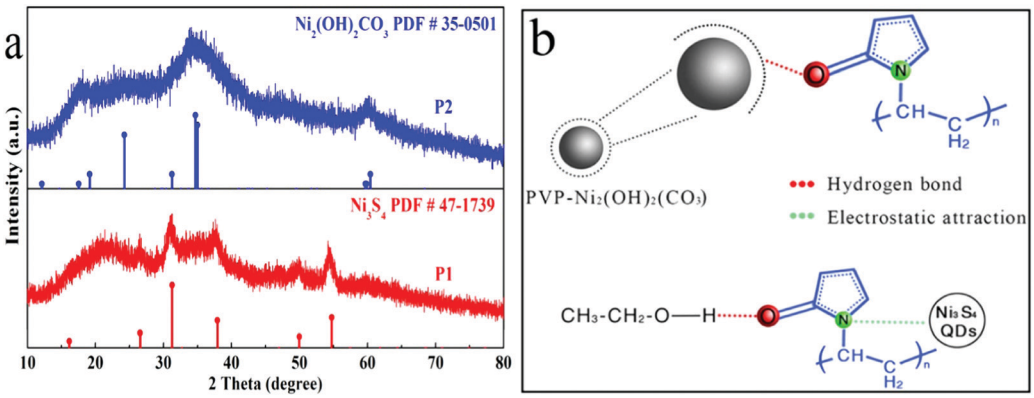

Fig. 1 (a) XRD patterns of P1 and P2, and (b) schematic illustration of the synergy between PVP and ethanol.

Among them, the peak of the XRD is broad due to the small size of the QDs. It's well known that Ni^{2+} (for example $Ni(OH)_2$, $NiCO_3$, NiO *etc.*) and S atoms are easily sulfided in the same system. However, the Ni^{2+} precursor with $S_2O_3^{2-}$ reacting in water medium was not sulfided but yielded P2 $Ni_2(OH)_2(CO_3)$. Here, we proposed a reaction mechanism, which is shown in Fig. 1b. Given urea has a lower decomposition temperature than $S_2O_3^{2-}$, urea-decomposed CO_3^{2-} and OH^- would first combine with Ni^{2+} to form $Ni_2(OH)_2(CO_3)$. Afterwards, the surface of $Ni_2(OH)_2(CO_3)$ adsorbs O atoms of PVP through hydrogen bonding, hindering $Ni_2(OH)_2(CO_3)$ being sulfurized by $S_2O_3^{2-}$.[30] By contrast, when ethanol was added to the solvent, ethanol and PVP formed hydrogen bonds, which blocked the adsorption between PVP and $Ni_2(OH)_2(CO_3)$ and facilitated the reaction between $Ni_2(OH)_2(CO_3)$ and $S_2O_3^{2-}$, finally resulting in Ni_3S_4. Also, the N atoms of PVP were electrostatically adsorbed on the surface of Ni_3S_4, which would prevent Ni_3S_4 agglomeration.[31] Moreover, due to the steric hindrance effect of N atoms, Ni_3S_4 wrapped with nitrogen could confine Ni_3S_4 to be QDs. The chemical reaction equations involved were as follows:[32,33]

$$CO(NH_2)_2 + 3H_2O \rightarrow 2NH_4^+ + CO_2 + 2OH^- \quad (R1)$$

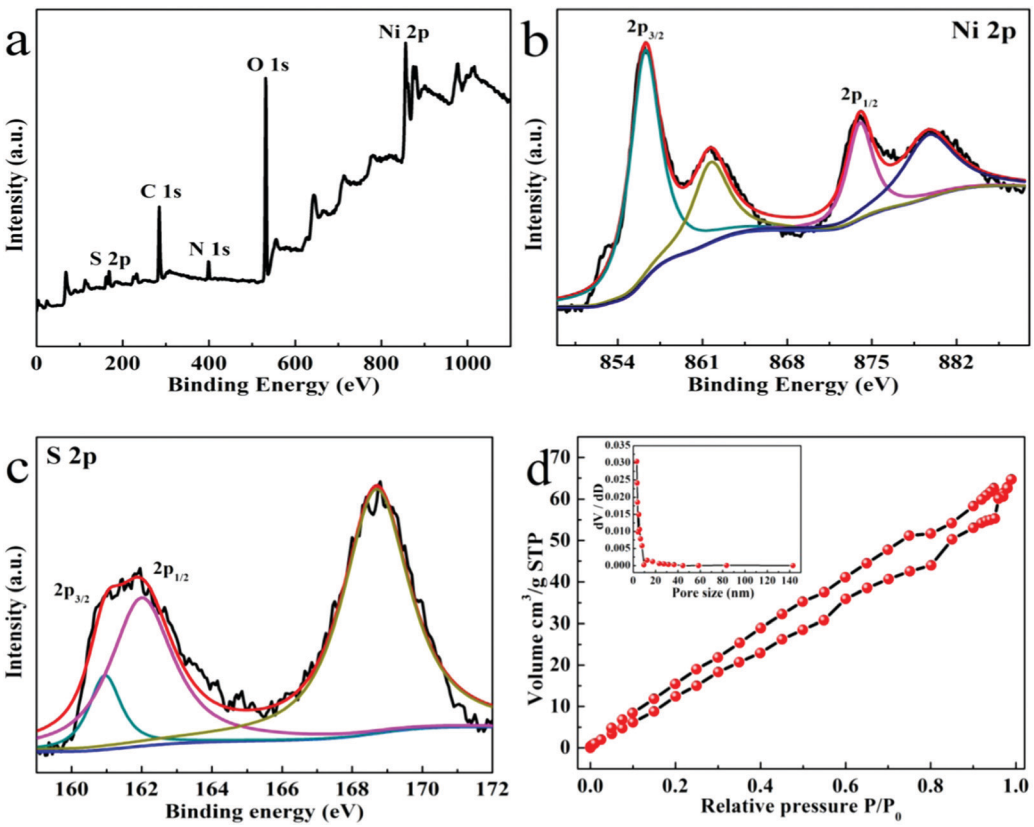

Fig. 2 (a–c) XPS: full survey scan spectrum, Ni, and S, and (d) nitrogen adsorption/desorption isotherms and BJH pore size distribution curves for Ni_3S_4 QDs.

$$CO_2 + 2OH^- \rightarrow CO_3^{2-} + H_2O \quad (R2)$$

$$Ni^{2+} + CO_3^{2-} + 2OH^- \rightarrow Ni_2(OH)_2(CO_3) \quad (R3)$$

$$Ni_2(OH)_2(CO_3) + 8S_2O_3^{2-} \rightarrow 2NiS + 6SO_4^{2-} + 8S + 2OH^- + CO_3^{2-} \quad (R4)$$

$$3NiS + S \rightarrow Ni_3S_4 \quad (R5)$$

XPS was used to detect the oxidation state of the elements of the Ni_3S_4 QDs. In the full scan spectrum of the sample (Fig. 2a), the elements Ni, S, C, N and O were detected. C, N and O were derived from air adsorption. The measured Ni/S atomic ratio was 3/4.4. In Fig. 2b, the binding energy of 856.3 eV and 874.1 eV indicated the presence of Ni^{2+}, and the binding energy of 861.8 eV and 879.9 eV indicated the presence of Ni^{3+}.[34,35] For the XPS spectrum of S 2p (Fig. 2c), the binding energies at 161 eV and 162.5 eV suggested the presence of Ni–S chemical bonds and S^{2-}. The binding energy at 168.7 eV was attributed to a high oxidation state of sulfur, such as $S_4O_6^{2-}$,[36] which could be due to the surface oxidization of Ni_3S_4 QDs by air.

Since the surface area and pore size distribution will affect the performance of the supercapacitor, a larger specific surface area will provide more active sites, and an appropriate pore size will facilitate the transmission and diffusion of electrolyte ions. Therefore, Ni_3S_4 QDs were tested for the nitrogen adsorption–desorption and pore size distribution as exhibited in Fig. 2d, which showed that the isotherms of the Ni_3S_4 QDs were type IV of the IUPAC classification, promoting the diffusion and transport of electrolyte ions.[37] The pore size distribution of the Ni_3S_4 QDs calculated by the BJH method shows that the pore size distribution was mainly below 5 nm. The measured BET surface area of the Ni_3S_4 QDs was 98.8 $m^2\ g^{-1}$, and the average pore diameter was 4 nm, demonstrating the great advance of Ni_3S_4 QDs as electrode materials.

The morphology of $Ni_2(OH)_2(CO_3)$ revealed by SEM showed a porous structure (Fig. 3a) which was due to the adsorption of PVP on the surface of $Ni_2(OH)_2(CO_3)$ preventing the agglomeration of the material. As displayed in Fig. 3b of the TEM image, Ni_3S_4 QDs of about 2–3 nm were well-dispersed, which was further verified by the inset of Fig. 3b. As can be seen, Ni_3S_4 QDs in ethanol dispersions showed no precipitation after being

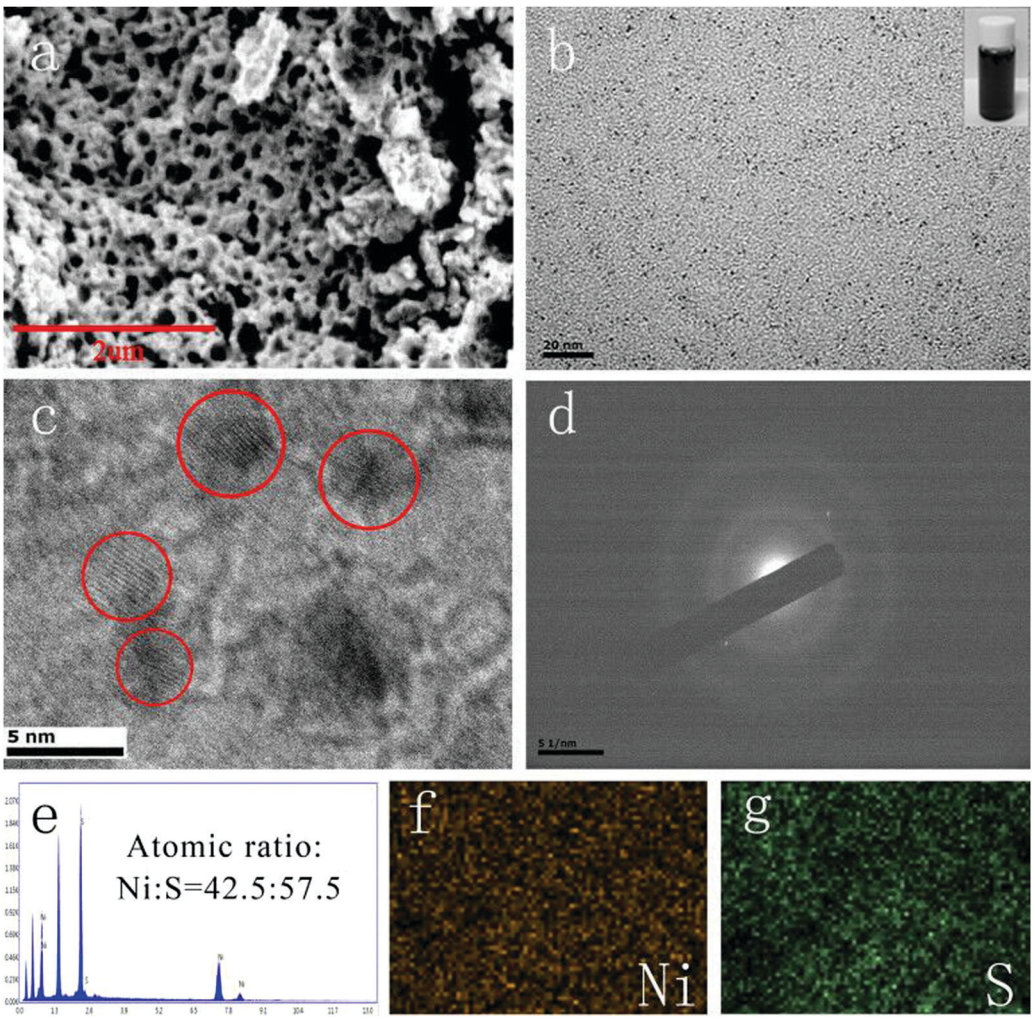

Fig. 3 (a) SEM image of $Ni_2(OH)_2(CO_3)$; Ni_3S_4 QDs: (b) TEM image, (c) HRTEM image, (d) SAED image, (e) EDS image, and (f and g) mapping patterns.

left for 1 month, indicating that the QDs have good stability. The HRTEM image of the Ni_3S_4 QDs (Fig. 3c) showed recognizable lattice fringes, suggesting good crystallinity, which was consolidated by the SAED image (Fig. 3d). The atomic molar ratio of Ni and S in the Ni_3S_4 QDs measured using the EDS spectrum (Fig. 3e) is 42.5 : 57.5, which was also consistent with XPS and the chemical formula. In Fig. 3f and g, the EDS mapping of the Ni_3S_4 QDs clearly showed the uniform distribution of Ni and S elements. According to the above test results, it was proved that this method can effectively synthesize Ni_3S_4 QDs.

3.2. Electrochemical properties of Ni_3S_4 QDs

The cyclic voltammetry (CV) curve of Fig. 4a shows the pseudocapacitor characteristics of the Ni_3S_4 QDs. At the same time, as the scan rate increased, the shape of the CV curve was basically unchanged, demonstrating the superior rate performance of the Ni_3S_4 QDs. According to the galvanostatic charge–discharge (GCD) curve of the Ni_3S_4 QDs (Fig. 4b), it can be seen that the Ni_3S_4 QD energy storage worked together with the electric double layer capacitance and the pseudocapacitance, but the specific capacitance contributed by the electric double layer capacitance was very small.[38] The specific capacitance of the Ni_3S_4 QDs was calculated according to Fig. 4b and eqn (1). When the current density was 1, 3, 5, 8, 10, 15, 20, and 25 A g^{-1}, the specific capacitance was 1440, 1213, 1085, 952, 882, 744, 628, and 500 F g^{-1}. The specific capacitance decrease with the increase of the current density was attributed to the fact that there was not enough time for the redox reaction. Fig. 4c shows the electrochemical impedance spectroscopy (EIS) spectra of the Ni_3S_4 QDs, and the inset is the equivalent circuit diagram (frequency range: 1–10^5 Hz, potential amplitude: 5 mV). It can be seen from the figure that the charge transfer resistance of the Ni_3S_4 QDs was very small at only 0.71 Ω. The slope of the Ni_3S_4 QDs was the largest in the low frequency region, which indicated that the surface diffusion rate of the electrolyte on the QDs was fast due to the large specific surface area of the QDs.[39] Fig. 4d shows the cycle stability test results of the Ni_3S_4 QDs at 10 A g^{-1}. As the number of cycles increased, the specific capacitance of the material gradually decreased. After 10k tests, the specific capacitance of the Ni_3S_4 QDs was maintained at 78% of the initial capacity, suggesting excellent cycle stability. Furthermore, the cycle performance of the prepared Ni_3S_4 QDs was compared with previously reported work as follows: $CoNi_2S_4$ (49%, 2000 cycles at 4 A g^{-1}),[40] $Zn_{0.76}Co_{0.24}S$ (86.4%, 2000 cycles at 5 A g^{-1}),[41] $CuCo_2S_4$ (90.1%, 5000 cycles at 3 A g^{-1}),[42] NiS/CoS/$NiCo_2S_4$ (60%, 500 cycles at 5 mV s^{-1}),[43] and CoS (95%, 1300 cycles at 10 A g^{-1}).[44] The Ni_3S_4 QDs exhibited obvious advantages of a larger number of cycles and longer service life. According to the above analysis, PVP and ethanol induced Ni_3S_4 QDs are excellent electrode materials for supercapacitors.

3.3. Electrochemical performance of the Ni_3S_4 QD//AC-ASC

As is known, an ASC can help increase the voltage range and energy density. To make Ni_3S_4 QDs convenient for practical

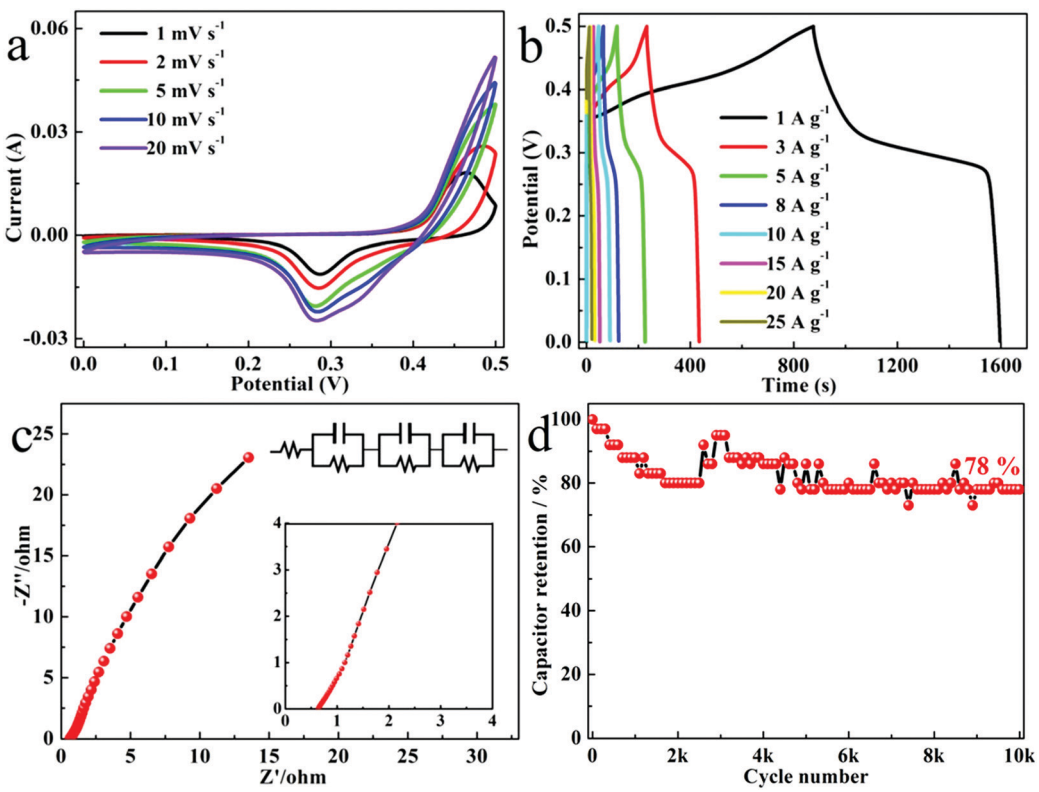

Fig. 4 Ni_3S_4 QDs: (a) CV curve, (b) GCD curve, (c) Nyquist plot of EIS, and (d) cyclic stability.

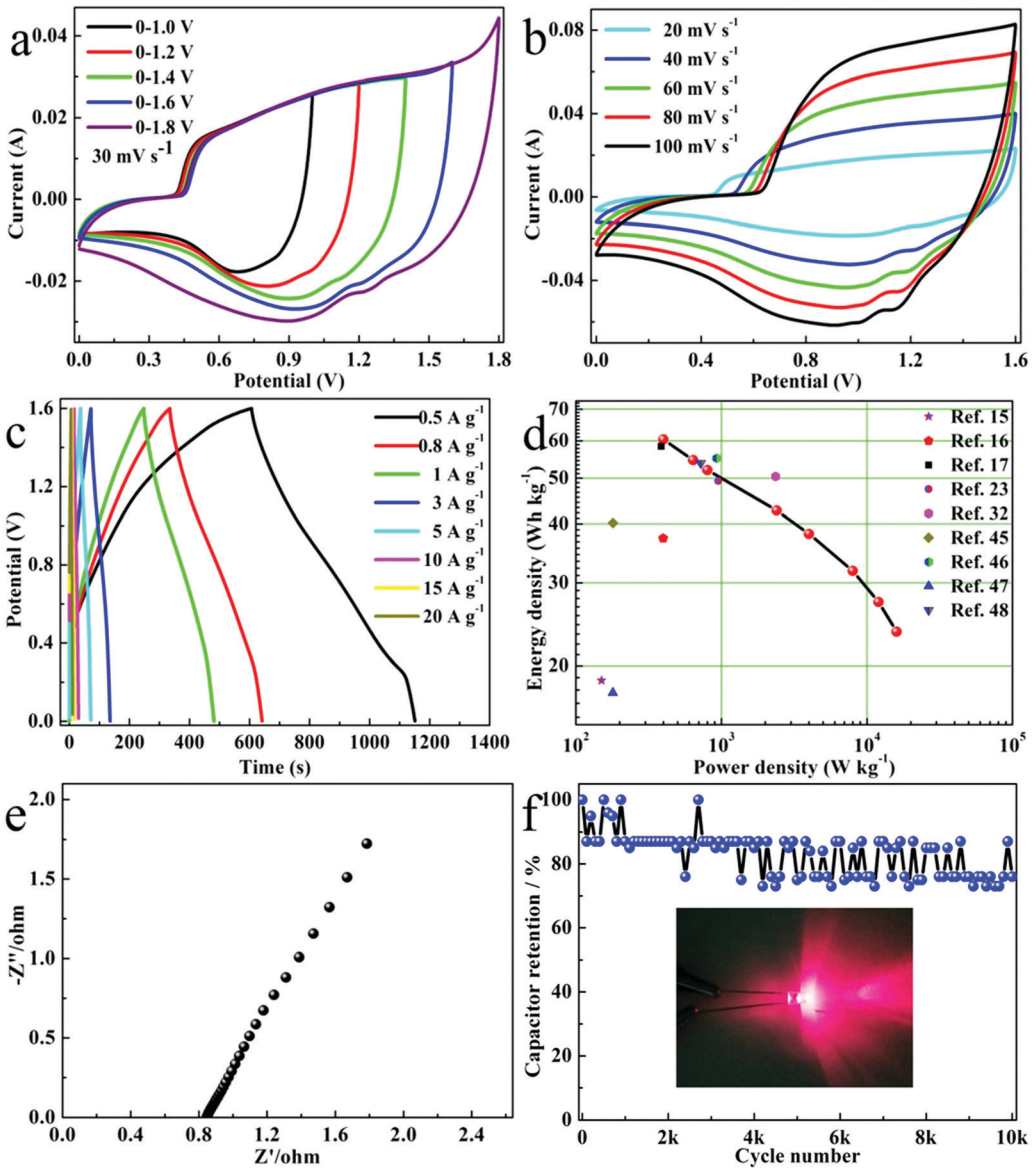

Fig. 5 Ni_3S_4 QD//AC-ASC: (a) CV curve in different voltage ranges, (b) CV curve with different scan rates, (c) GCD curve, (d) relationship between the energy density and power density, (e) EIS spectrum and (f) cyclic stability.

applications, a Ni_3S_4 QD//AC-ASC was assembled using Ni_3S_4 QDs and AC as the positive and negative electrodes, and tested in a 6 M KOH solution. AC (YEC-8A) was purchased from Fuzhou Yihuan Carbon Co., Ltd, China. The mass ratio of the positive electrode and the negative electrode was determined according to eqn (2). In fact, the essence of eqn (2) is charge balance theory and the calculated $m(Ni_3S_4\ QDs) : m(AC) = 1 : 2.2$. As shown in Fig. 5a of the CV curves of the ASC in different voltage ranges, the ASC can stably expand to 1.6 V. When it was greater than 1.6 V, electrochemical polarization would occur, manifested by electrolyzed water and bubbles. Based on the non-rectangular CV curve of the ASC (Fig. 5b), it can be seen that the reactions are mainly redox reactions. When the scan rate increased, the shape of the CV curve didn't change, indicating good rate performance. The symmetrical GCD curve (Fig. 5c) showed that the ASC had high Coulombic efficiency. As shown in Fig. 5d of the energy density and power density calculated from eqn (3) and (4) and the GCD curves, the ASC had a power density of 400 W kg^{-1} at an energy density of 60.4 W h kg^{-1}. Even when the power density was 16 kW kg^{-1}, the energy density can still maintain 23.6 W h kg^{-1}. The performance of our assembled ASC devices was superior to many previously reported nickel sulfide ASCs, such as Ni_3S_4//AC,[15] Ni_3S_4@rGO-20//rGO,[16] Ni_3S_4-MoS_2//AC,[17] Ni_3S_4 QD/NF//AC/NF,[23] TRGO//NCC2,[32] NG/Ni-S-1//AC,[45] Ni_3S_2@β-NiS//AC,[46] Ni_3S_2@PPy//AC,[47] and Co^{2+} doped Ni_3S_4//AC.[48] Fig. 5e shows the EIS spectrum of the ASC (frequency range: 1–10^5 Hz, potential amplitude: 5 mV), which showed that the equivalent series resistance was only 0.85 Ω, indicating that the internal resistance and charge transfer resistance of the ASC are very

low, which is conducive to electron transport. In order to evaluate whether the ASC device can be used for a long time, we performed 10k constant current charge and discharge cycle tests under a voltage window of 1.6 V and a current density of 10 A g^{-1}. As shown in Fig. 5f, the specific capacitance kept 76% of the initial value, indicating that the ASC has good cycle stability, which was compared with the previously reported work as follows: Ni_3S_4//AC (93%, 5000 cycles at 2 A g^{-1}),[15] TRGO//NCC2 (83%, 6000 cycles at 12 A g^{-1}),[32] 3DNC@$MnCo_2S_4$//AC (82%, 5000 cycles at 10 A g^{-1}),[49] $CuCo_2S_4$/GA//AC (70.4%, 5000 cycles at 2 A g^{-1}),[50] $NiCo_2S_4$/GA//AC (71.6%, 5000 cycles at 2 A g^{-1}),[51] and $ZnCo_2S_4$//AC (98.7%, 2000 cycles at 6 A g^{-1}).[52] Two ASC devices connected in series can successfully illuminate an LED light, which can be well applied in practice. Considering the simple and environmentally-friendly synthesis method and its high energy density, our synthesis method holds great promise in the application of high energy storage devices.

4. Conclusions

In summary, by taking advantage of the synergy of PVP and ethanol, we facilely synthesized Ni_3S_4 QDs, during which the whole process not only did not require nitrogen protection but also was environmentally-friendly. In addition, insight into the synergistic mechanism was explored. When Ni_3S_4 QDs were used as the electrode material, they delivered a high specific capacitance of 1440 F g^{-1} at 1 A g^{-1} and superior cycle stability. The ASC with Ni_3S_4 QDs as the positive electrode and AC as the negative electrode showed a high energy density of 60.4 W h kg^{-1} at a power density of 400 W kg^{-1}, which successfully drove an electronic device, demonstrating that the as-synthesized Ni_3S_4 QDs witnessed great advances for supercapacitors. This work provides a simple and environmentally-friendly method for designing metal-sulfide QDs as electrode materials.

Conflicts of interest

There are no conflicts to declare.

Acknowledgements

This work was supported by the National Natural Science Foundation of China (Grant No. 51771001, 21471001 and 21575001); Independent Research and Development Project of Anhui Province (201904a07020001); and the Open Project of Key Laboratory of Structure and Functional Regulation of Hybrid Materials (Anhui University), Ministry of Education.

References

1 D.-W. Wang, F. Li and H.-M. Cheng, Hierarchical porous nickel oxide and carbon as electrode materials for asymmetric supercapacitor, *J. Power Sources*, 2008, **185**, 1563–1568.
2 R. F. Service, Lithium-ion battery development takes Nobel, *Science*, 2019, **366**, 292.
3 D. Castelvecchi and E. Stoye, Chemistry Nobel honours world-changing batteries, *Nature*, 2019, **574**, 308.
4 X. Hu, Z. Deng, J. Suo and Z. Pan, A high rate, high capacity and long life ($LiMn_2O_4$ + AC)/$Li_4Ti_5O_{12}$ hybrid battery–supercapacitor, *J. Power Sources*, 2009, **187**, 635–639.
5 N. W. Duffy, W. Baldsing and A. G. Pandolfo, The nickel–carbon asymmetric supercapacitor—Performance, energy density and electrode mass ratios, *Electrochim. Acta*, 2008, **54**, 535–539.
6 L.-l. Liu, K. P. Annamalai and Y.-s. Tao, A hierarchically porous $CuCo_2S_4$/graphene composite as an electrode material for supercapacitors, *New Carbon Mater.*, 2016, **31**, 336–342.
7 H. Tang, J. Wang, H. Yin, H. Zhao, D. Wang and Z. Tang, Growth of polypyrrole ultrathin films on MoS_2 monolayers as high-performance supercapacitor electrodes, *Adv. Mater.*, 2015, **27**, 1117–1123.
8 R. BoopathiRaja, M. Parthibavarman and A. Nishara Begum, Hydrothermal induced novel $CuCo_2O_4$ electrode for high performance supercapacitor applications, *Vacuum*, 2019, **165**, 96–104.
9 M. Chen, J. Wang, H. Tang, Y. Yang, B. Wang, H. Zhao and D. Wang, Synthesis of multi-shelled MnO_2 hollow microspheres via an anion-adsorption process of hydrothermal intensification, *Inorg. Chem. Front.*, 2016, **3**, 1065–1070.
10 J. Cao, Q. Mei, R. Wu and W. Wang, Flower-like nickel–cobalt layered hydroxide nanostructures for super long-life asymmetrical supercapacitors, *Electrochim. Acta*, 2019, **321**, 134711.
11 D. A. L. Almeida and N. G. Ferreira, Fabrication of binary composites from polyaniline deposits on carbon fibers heat treated at three different temperatures: structural and electrochemical analyses for potential application in supercapacitors, *Mater. Chem. Phys.*, 2020, **239**, 122101.
12 A. M. Saleem, R. Andersson, V. Desmaris and P. Enoksson, Integrated on-chip solid state capacitor based on vertically aligned carbon nanofibers, grown using a CMOS temperature compatible process, *Solid-State Electron.*, 2018, **139**, 75–79.
13 J. Du, Q. Yan, Y. Li, K. Cheng, K. Ye, K. Zhu, J. Yan, D. Cao, X. Zhang and G. Wang, Hierarchical copper cobalt sulfides nanowire arrays for high-performance asymmetric supercapacitors, *Appl. Surf. Sci.*, 2019, **487**, 198–205.
14 M. Chuai, K. Zhang, X. Chen, Y. Tong, H. Zhang and M. Zhang, Effect of nondegeneracy on $Ni_{3-x}Co_xS_4$ for high performance supercapacitor, *Chem. Eng. J.*, 2020, **381**, 122682.
15 H. Wang, M. Liang, D. Duan, W. Shi, Y. Song and Z. Sun, Rose-like Ni_3S_4 as battery-type electrode for hybrid supercapacitor with excellent charge storage performance, *Chem. Eng. J.*, 2018, **350**, 523–533.
16 Q. Hu, X. Zou, Y. Huang, Y. Wei, Ya Wang, F. Chen, B. Xiang, Q. Wu and W. Li, Graphene oxide-drove transformation of NiS/Ni_3S_4 microbars towards Ni_3S_4 polyhedrons for supercapacitor, *J. Colloid Interface Sci.*, 2019, **559**, 115–123.

17 W. Luo, G. Zhang, Y. Cui, Y. Sun, Q. Qin, J. Zhang and W. Zheng, One-step extended strategy for the ionic liquid-assisted synthesis of Ni_3S_4–MoS_2 heterojunction electrodes for supercapacitors, *J. Mater. Chem. A*, 2017, **5**, 11278–11285.
18 J. Wang, H. Tang, H. Ren, R. Yu, J. Qi, D. Mao, H. Zhao and D. Wang, pH-Regulated Synthesis of Multi-Shelled Manganese Oxide Hollow Microspheres as Supercapacitor Electrodes Using Carbonaceous Microspheres as Templates, *Adv. Sci.*, 2014, **1**, 1400011.
19 L. Tan, Z. Su, R. Yang, J. Tao, D. Zhao, Z. Zhang and F. Wen, Oxygen evolution catalytic performance of quantum dot nickel-iron double hydroxide/reduced graphene oxide composites, *Mater. Lett.*, 2018, **231**, 24–27.
20 F. Hasanpour, M. Nekoeinia, A. Semnani and S. Shojaei, $NiMnO_3$ nanoparticles anchored on graphene quantum dot: Application in sensitive electroanalysis of dobutamine, *Microchem. J.*, 2018, **142**, 17–23.
21 T. K. Nideep, M. Ramya, V. P. N. Nampoori and M. Kailasnath, The size dependent thermal diffusivity of water soluble CdTe quantum dots using dual beam thermal lens spectroscopy, *Phys. E*, 2020, **116**, 113724.
22 W. Chen, X. Zhang, L.-E. Mo, Z. Feng, S. Chen, X. Zhang, Y. Zhang and L. Hu, Ligands induced NiS_2 quantum dots for synchronous high specific capacity and robust stability of advanced electrochemical energy storage, *Chem. Eng. J.*, 2019, **375**, 121981.
23 W. Chen, X. Zhang, Y. Peng, L.-E. Mo, Z. Li, Y. Zhang, X. Zhang and L. Hu, One-pot scalable synthesis of pure phase Ni_3S_4 quantum dots as a versatile electrode for high performance hybrid supercapacitors and lithium ion batteries, *J. Power Sources*, 2019, **438**, 227004.
24 F. Xue, M. Liu, C. Cheng, J. Deng and J. Shi, Localized NiS_2 Quantum Dots on g-C_3N_4 Nanosheets for Efficient Photocatalytic Hydrogen Production from Water, *ChemCatChem*, 2018, **10**, 5441–5448.
25 N. K. Toru Takagishi, Interaction of Polyvinylpyrrolidone with Methyl Orange and Its Homologs in Aqueous Solution: Thermodynamics of the Binding Equilibria and Their Temperature Dependences, *J. Polym. Sci., Polym. Chem. Ed.*, 1973, **11**, 1889–1900.
26 H. Wang, J. Yan, R. Wang, S. Li, D. J. L. Brett, J. Key and S. Ji, Toward high practical capacitance of $Ni(OH)_2$ using highly conductive CoB nanochain supports, *J. Mater. Chem. A*, 2017, **5**, 92–96.
27 H. T. T. Thanh, P. A. Le, M. D. Thi, T. Le Quang and T. N. Trinh, Effect of gel polymer electrolyte based on polyvinyl alcohol/polyethylene oxide blend and sodium salts on the performance of solid-state supercapacitor, *Bull. Mater. Sci.*, 2018, **41**, 145.
28 B. J. Reddy, P. Vickraman and A. S. Justin, Asymmetric supercapacitor device performance based on microwave synthesis of N-doped graphene/nickel sulfide nanocomposite, *J. Mater. Sci.*, 2019, **54**, 6361–6373.
29 U. Evariste, G. Jiang, B. Yu, Y. Liu and P. Ma, Electrodeposition of Manganese-Nickel-Cobalt Sulfides on Reduced Graphene Oxide/Nickel Foam for High-Performance Asymmetric Supercapacitors, *J. Electron. Mater.*, 2020, **49**(2), 922–930.
30 G. Wang, Y. Ma, J. Mu, Z. Zhang, X. Zhang, L. Zhang, H. Che, Y. Bai, J. Hou and H. Xie, Monodisperse polyvinylpyrrolidone-coated $CoFe_2O_4$ nanoparticles: Synthesis, characterization and cytotoxicity study, *Appl. Surf. Sci.*, 2016, **365**, 114–119.
31 S. Kumari, A. A. Khan, A. Chowdhury, A. K. Bhakta, Z. Mekhalif and S. Hussain, Efficient and highly selective adsorption of cationic dyes and removal of ciprofloxacin antibiotic by surface modified nickel sulfide nanomaterials: Kinetics, isotherm and adsorption mechanism, *Colloids Surf., A*, 2019, 124264.
32 S. Ghosh, J. Sharath Kumar, N. Chandra Murmu, R. Sankar Ganesh, H. Inokawa and T. Kuila, Development of carbon coated NiS_2 as positive electrode material for high performance asymmetric supercapacitor, *Composites, Part B*, 2019, **177**, 107373.
33 S. Liu, K. S. Hui, K. N. Hui, V. V. Jadhav, Q. X. Xia, J. M. Yun, Y. R. Cho, R. S. Mane and K. H. Kim, Facile Synthesis of Microsphere Copper Cobalt Carbonate Hydroxides Electrode for Asymmetric Supercapacitor, *Electrochim. Acta*, 2016, **188**, 898–908.
34 F. Chen, H. Wang, S. Ji, V. Linkov and R. Wang, Core–shell structured Ni_3S_2@$Co(OH)_2$ nano-wires grown on Ni foam as binder-free electrode for asymmetric supercapacitors, *Chem. Eng. J.*, 2018, **345**, 48–57.
35 Y. Shen, K. Zhang, B. Chen, F. Yang, K. Xu and X. Lu, Enhancing the electrochemical performance of nickel cobalt sulfides hollow nanospheres by structural modulation for asymmetric supercapacitors, *J. Colloid Interface Sci.*, 2019, **557**, 135–143.
36 F. Wang, J. Zheng, J. Ma, K. Zhou and Q. Wang, One-step facile route to glucose/copper cobalt sulfide nanorod for high-performance asymmetric supercapacitors, *J. Nanopart. Res.*, 2019, **21**, 189.
37 B. Duan, X. Gao, X. Yao, Y. Fang, L. Huang, J. Zhou and L. Zhang, Unique elastic N-doped carbon nanofibrous microspheres with hierarchical porosity derived from renewable chitin for high rate supercapacitors, *Nano Energy*, 2016, **27**, 482–491.
38 L. Xie, Z. Hu, C. Lv, G. Sun, J. Wang, Y. Li, H. He, J. Wang and K. Li, Co_xNi_{1-x} double hydroxide nanoparticles with ultrahigh specific capacitances as supercapacitor electrode materials, *Electrochim. Acta*, 2012, **78**, 205–211.
39 T. K. Enock, C. K. King'ondu, A. Pogrebnoi and Y. A. C. Jande, Biogas-slurry derived mesoporous carbon for supercapacitor applications, *Mater. Today Energy*, 2017, **5**, 126–137.
40 W. Du, Z. Zhu, Y. Wang, J. Liu, W. Yang, X. Qian and H. Pang, One-step synthesis of $CoNi_2S_4$ nanoparticles for supercapacitor electrodes, *RSC Adv.*, 2014, **4**, 6998.
41 J. Yang, Y. Zhang, C. Sun, G. Guo, W. Sun, W. Huang, Q. Yan and X. Dong, Controlled synthesis of zinc cobalt sulfide nanostructures in oil phase and their potential applications in electrochemical energy storage, *J. Mater. Chem. A*, 2015, **3**, 11462–11470.
42 Y. Zhu, X. Ji, H. Chen, L. Xi, W. Gong and Y. Liu, The investigation of the electrochemically supercapacitive

performances of mesoporous $CuCo_2S_4$, *RSC Adv.*, 2016, **6**, 84236–84241.

43 D. Li, X. Zhang, L. Pei, C. Dong, J. Shi and Y. Xu, High-performance supercapacitors and non-enzymatic electrochemical glucose sensor based on tremella-like NiS/CoS/$NiCo_2S_4$ hierarchical structure, *Inorg. Chem. Commun.*, 2019, **110**, 107581.

44 J. Li, D. Chen and Q. Wu, Facile synthesis of CoS porous nanoflake for high performance supercapacitor electrode materials, *J. Energy Storage*, 2019, **23**, 511–514.

45 Y. Luo, W. Que, C. Yang, Y. Tian, Y. Yang and X. Yin, Nitrogen-doped graphene/multiphase nickel sulfides obtained by Ni-$C_3N_3S_3$ (metallopolymer) assisted synthesis for high-performance hybrid supercapacitors, *Electrochim. Acta*, 2019, **301**, 332–341.

46 W. Li, S. Wang, L. Xin, M. Wu and X. Lou, Single-crystal β-NiS nanorod arrays with a hollow-structured Ni_3S_2 framework for supercapacitor applications, *J. Mater. Chem. A*, 2016, **4**, 7700–7709.

47 L. Long, Y. Yao, M. Yan, H. Wang, G. Zhang, M. Kong, L. Yang, X. Liao, G. Yin and Z. Huang, Ni_3S_2@polypyrrole composite supported on nickel foam with improved rate capability and cycling durability for asymmetric supercapacitor device applications, *J. Mater. Sci.*, 2016, **52**, 3642–3656.

48 Y. Li, J. Li, M. Wang, Y. Liu and H. Cui, High rate performance and stabilized cycle life of Co^{2+}-doped nickel sulfide nanosheets synthesized by a scalable method of solid-state reaction, *Chem. Eng. J.*, 2019, **366**, 33–40.

49 M. Hua, F. Cui, Y. Huang, Y. Zhao, J. Lian, J. Bao, B. Zhang, S. Yuan and H. Li, Crafting nanosheet-built $MnCo_2S_4$ disks on robust N-doped carbon matrix for hybrid supercapacitors, *Electrochim. Acta*, 2019, **323**, 134770.

50 Z. Tian, X. Wang, B. Li, H. Li and Y. Wu, High rate capability electrode constructed by anchoring $CuCo_2S_4$ on graphene aerogel skeleton toward quasi-solid-state supercapacitor, *Electrochim. Acta*, 2019, **298**, 321–329.

51 B. Li, Z. Tian, H. Li, Z. Yang, Y. Wang and X. Wang, Self-supporting graphene aerogel electrode intensified by $NiCo_2S_4$ nanoparticles for asymmetric supercapacitor, *Electrochim. Acta*, 2019, **314**, 32–39.

52 C. Cheng, X. Zhang, C. Wei, Y. Liu, C. Cui, Q. Zhang and D. Zhang, Mesoporous hollow $ZnCo_2S_4$ core–shell nanospheres for high performance supercapacitors, *Ceram. Int.*, 2018, **44**, 17464–17472.

